RESEARCH ARTICLE

Gut Microbiota Promotes Obesity-Associated Liver Cancer through PGE_2-Mediated Suppression of Antitumor Immunity

Tze Mun Loo[1], Fumitaka Kamachi[1], Yoshihiro Watanabe[1], Shin Yoshimoto[2,3], Hiroaki Kanda[4], Yuriko Arai[1,2], Yaeko Nakajima-Takagi[5], Atsushi Iwama[5], Tomoaki Koga[6], Yukihiko Sugimoto[6], Takayuki Ozawa[1], Masaru Nakamura[1], Miho Kumagai[1], Koichi Watashi[7,8], Makoto M. Taketo[9], Tomohiro Aoki[10], Shuh Narumiya[10,11,12], Masanobu Oshima[12,13], Makoto Arita[14,15,16,17], Eiji Hara[2,12,18], and Naoko Ohtani[1,16]

ABSTRACT

Obesity increases the risk of cancers, including hepatocellular carcinomas (HCC). However, the precise molecular mechanisms through which obesity promotes HCC development are still unclear. Recent studies have shown that gut microbiota may influence liver diseases by transferring its metabolites and components. Here, we show that the hepatic translocation of obesity-induced lipoteichoic acid (LTA), a Gram-positive gut microbial component, promotes HCC development by creating a tumor-promoting microenvironment. LTA enhances the senescence-associated secretory phenotype (SASP) of hepatic stellate cells (HSC) collaboratively with an obesity-induced gut microbial metabolite, deoxycholic acid, to upregulate the expression of SASP factors and COX2 through Toll-like receptor 2. Interestingly, COX2-mediated prostaglandin E_2 (PGE_2) production suppresses the antitumor immunity through a PTGER4 receptor, thereby contributing to HCC progression. Moreover, COX2 overexpression and excess PGE_2 production were detected in HSCs in human HCCs with noncirrhotic, nonalcoholic steatohepatitis (NASH), indicating that a similar mechanism could function in humans.

SIGNIFICANCE: We showed the importance of the gut–liver axis in obesity-associated HCC. The gut microbiota–driven COX2 pathway produced the lipid mediator PGE_2 in senescent HSCs in the tumor microenvironment, which plays a pivotal role in suppressing antitumor immunity, suggesting that PGE_2 and its receptor may be novel therapeutic targets for noncirrhotic NASH-associated HCC. *Cancer Discov; 7(5); 522–38. ©2017 AACR.*

[1]Department of Applied Biological Science, Faculty of Science and Technology, Tokyo University of Science, Chiba, Japan. [2]Division of Cancer Biology, Cancer Institute, Japanese Foundation for Cancer Research, Tokyo, Japan. [3]LSI Medience Corporation, Tokyo, Japan. [4]Division of Pathology, Cancer Institute, Japanese Foundation for Cancer Research, Tokyo, Japan. [5]Department of Cellular and Molecular Medicine, Graduate School of Medicine, Chiba University, Chiba, Japan. [6]Department of Pharmaceutical Biochemistry, Graduate School of Pharmaceutical Sciences, Kumamoto University, Kumamoto, Japan. [7]Department of Virology II, National Institute of Infectious Diseases, Tokyo, Japan. [8]CREST, Japan Science and Technology Agency (JST), Saitama, Japan. [9]Department of Pharmacology, Graduate School of Medicine, Kyoto University, Yoshida-Konoé-cho, Kyoto, Japan. [10]Center for Innovation in Immunoregulation Technology and Therapeutics, Kyoto University Graduate School of Medicine, Konoe-cho Yoshida, Kyoto, Japan. [11]Medical Innovation Center, Kyoto University Graduate School of Medicine, Kyoto, Japan. [12]AMED-CREST, AMED, Japan Agency for Medical Research and Development, Tokyo, Japan. [13]Division of Genetics, Cancer Research Institute, Kanazawa University, Kanazawa, Japan. [14]Laboratory for Metabolomics, RIKEN Center for Integrative Medical Sciences, Kanagawa, Japan. [15]Graduate School of Medical Life Science, Yokohama City University, Kanagawa, Japan. [16]PRESTO, Japan Science and Technology Agency, Kawaguchi, Saitama, Japan. [17]Division of Physiological Chemistry and Metabolism, Graduate School of Pharmaceutical Sciences, Keio University, Tokyo, Japan. [18]Department of Molecular Microbiology, Research Institute for Microbial Diseases, Osaka University, Osaka, Japan.

Note: Supplementary data for this article are available at Cancer Discovery Online (http://cancerdiscovery.aacrjournals.org/).

Current address for N. Ohtani: Department of Pathophysiology, Osaka City University, Graduate School of Medicine, Osaka, Japan.

Corresponding Author: Naoko Ohtani, Department of Pathophysiology, Osaka City University, Graduate School of Medicine, Asahimachi 1-4-3, Abeno-ku, Osaka, 545-8585, Japan. Phone: 81-6-6645-3710; Fax: 81-6-6645-3712; E-mail: ohtani.naoko@med.osaka-cu.ac.jp

doi: 10.1158/2159-8290.CD-16-0932

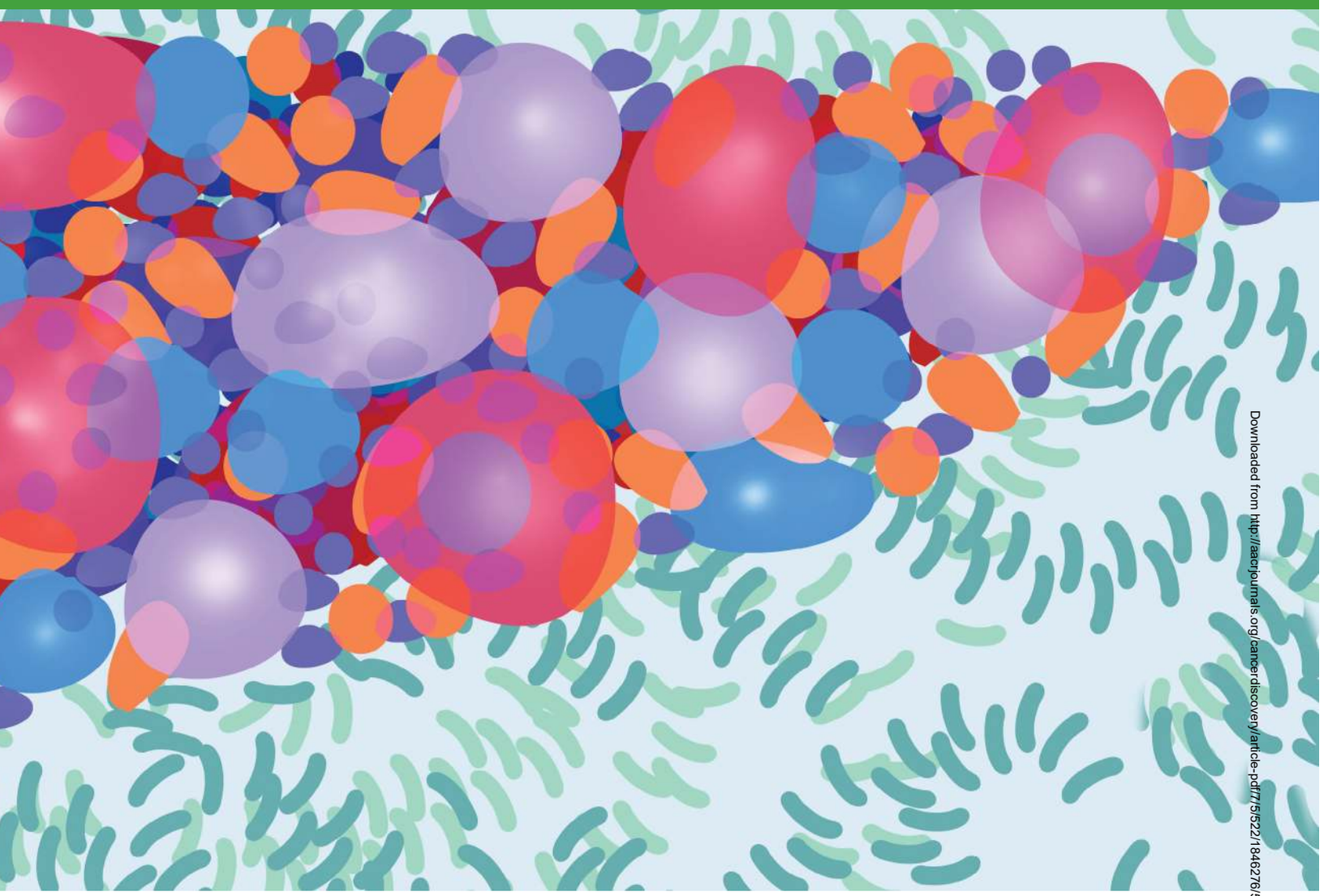

INTRODUCTION

Obesity has become a worldwide health problem and is known to increase the risk of diabetes, cardiovascular disease, and several types of cancer (1). Although hypernutrition-related systemic alterations are thought to be involved in cancer development (2–4), the molecular mechanisms that integrate these events still remain largely unclear. Among obesity-associated cancers, liver cancer has been shown to have a strong relationship with obesity, based on epidemiological studies (1). The most common risk factor for hepatocellular carcinoma (HCC) is long-term infection by hepatitis B virus (HBV) or hepatitis C virus (HCV; ref. 5). However, obesity-associated nonalcoholic fatty liver disease (NAFLD) and nonalcoholic steatohepatitis (NASH) have recently emerged as important risk factors for liver cancer (6). Therefore, elucidation of the precise molecular mechanisms mediating the development of obesity-induced NASH-associated HCC is urgently needed.

We previously reported that increased enterohepatic circulation of the obesity-induced Gram-positive gut microbial metabolite deoxycholic acid (DCA) facilitates HCC development by inducing cellular senescence and the senescence-associated secretory phenotype (SASP) in hepatic stellate cells (HSC) in the tumor microenvironment. This recently identified phenotype of senescent cells involves secretion of a series of inflammatory cytokines, chemokines, matrix-remodeling factors, and growth factors (7), suggesting that the gut–liver axis plays a pivotal role in inducing cellular senescence of HSCs and liver tumorigenesis (4). The importance of the SASP phenotype has also been recognized *in vivo* in a variety of pathophysiologic contexts, giving rise to not only deleterious effects such as chronic inflammation and tumorigenesis (4, 8, 9), but also beneficial effects such as embryonal development (10, 11), immunosurveillance (12–14), and tissue repair (15, 16), depending on the biological context. Indeed, the paracrine effects of SASP have been reported to be dependent on the surrounding cells (17), particularly on the p53 status of these cells (18). Accumulating evidence has indicated that SASP is regulated by a combination of several transcription factors, epigenetic regulators, and metabolic pathways, in response to DNA damage (19–23). DCA can create DNA

damage by elevating the levels of reactive oxygen species (ROS), thereby inducing cellular senescence and the SASP to promote obesity-associated HCC (4). However, the trigger that initiates the SASP signals may vary depending on physiologic status, and thus the precise mechanisms regulating the expression of SASP factors need to be elucidated in each pathophysiologic setting (24).

One of the mechanisms that may trigger the SASP could be Toll-like receptor (TLR) signaling. High mobility group box 1 (HMGB1) activates TLR4-mediated cytokine signals in an autocrine manner in senescent cells (25). In addition, previous *in vivo* studies have demonstrated that TLR4-mediated inflammatory signals induced by the Gram-negative bacterial component lipopolysaccharide (LPS) are important for promoting liver fibrosis and fibrosis-associated liver tumorigenesis (26). However, in our obesity-associated HCC model, Gram-positive bacteria, but not Gram-negative bacteria, were found to be dramatically increased in obese mice fed a high-fat diet (HFD; ref. 4), consistent with previous reports (27). Moreover, we did not observe the reduction of obesity-associated liver tumor formation in TLR4-deficient mice as compared with those in wild-type mice when we performed the same protocol of neonatal 7,12-dimethylbenz(*a*)anthracene (DMBA) treatment with HFD (4), suggesting that TLR4-mediated signals are unlikely to be involved in the acceleration of obesity-associated HCC in our experimental setting.

In this study, we investigated the effects of the signals by lipoteichoic acid (LTA), a cell wall component from Gram-positive bacteria, on the induction of the SASP factors in DCA-induced senescent HSCs and on obesity-associated liver tumor development. We newly identified that a gut microbiota–driven COX2 pathway generated the lipid mediator prostaglandin E_2 (PGE_2), which functioned as a key SASP factor in the tumor microenvironment. Our current study provides important mechanistic insights into the relevance of the gut–liver axis in obesity-associated liver carcinogenesis.

RESULTS

A Normal Diet Delays Liver Carcinogenesis Compared with an HFD

We previously reported that neonatal DMBA treatment in HFD-fed mice resulted in development of HCC within 30 weeks, and demonstrated that DCA, an obesity-associated gut microbial metabolite, is a critical factor promoting obesity-associated HCC development (4). To further define the role of DCA itself, DMBA-treated mice were fed DCA with a normal diet (ND; Fig. 1A). DCA administration in ND-fed mice did not induce HCC development at 30 weeks, at which point HFD-fed mice exhibited HCC with sufficient body-weight gain (Fig. 1B–D). Senescence markers, such as upregulation of p21 and the DNA damage response marker 53BP1, were detected in HSCs in the livers of mice fed DCA and an ND, reaching levels similar to those in the livers of HFD-fed mice at 30 weeks (Fig. 1E). However, at this time point, the frequency of SASP induction in HSCs was much lower in livers from mice fed DCA and an ND as compared with that in mice fed an HFD (Fig. 1E, IL1β, Groα, and IL6). We found that mice fed DCA and an ND required approximately six more months for complete SASP induction and HCC development at the 55-week time point (Fig. 1B–E). Therefore, we speculated that other factors underlying the HFD-fed obese liver could be necessary to accelerate the effects of DCA in aggressively promoting HCC development. Accordingly, we searched for factors that promote obesity-associated HCC progression, based on (i) the obesity-induced gut microbial component(s) and (ii) the increased lipid storage in the liver tumor areas of HFD-fed obese mice.

LTA- and TLR2-Mediated Signaling Promotes Obesity-Associated HCC Development

When we reanalyzed the gut microbial profiles of DMBA-treated mice, we again noted that HFD-fed mice exhibited a dramatic increase in Gram-positive gut microbiota in their feces (Supplementary Fig. S1; refs. 4, 27). The gut microbial overgrowth and increased hepatic translocation of the gut microbial components and metabolites from the intestine, the so-called gut–liver axis, are known to play a role in the pathogenesis of liver disorders (26, 28). We therefore examined whether LTA, a major cell wall component in Gram-positive bacteria, accumulated in the livers of DMBA-treated and HFD-fed mice. We found relatively high amounts of LTA accumulation in the areas of the liver tumors (Fig. 2A). Because LTA is a major ligand of the innate immunity receptor TLR2, we next investigated the involvement of TLR2-mediated signaling in liver tumor development. Interestingly, both the numbers and sizes of HFD-induced liver tumors were strikingly reduced in TLR2-deficient mice, although body weights were not different between the two groups (Fig. 2B–E). Accordingly, in livers from TLR2-deficient mice, the expression of SASP factors, such as IL1β, Groα, and IL6, was significantly reduced in HSCs, suggesting that TLR2-mediated signaling induced the expression of SASP factors (Fig. 2F). Notably, however, the presence of p21 and 53BP1 foci was still observed in activated HSCs from TLR2-deficient mice (Fig. 2F). The majority of senescent signals are detected in the HSCs but not in HCC cells in the tumor region (Supplementary Fig. S2). Taken together, these results suggest that TLR2-mediated signaling is important for the upregulation of SASP factors in senescent HSCs but not for the induction of senescent cell-cycle arrest.

Figure 1. DCA administration with ND induced a long delay in liver carcinogenesis as compared with HFD. **A,** Timeline of the experimental procedure (ND, $n = 3$; ND + DCA 30 weeks, $n = 3$; ND + DCA 55 weeks, $n = 5$; HFD, $n = 15$). Eut, euthanasia. **B,** The average body weight of each group at the indicated age. Data, means ± SD. **, $P < 0.01$. D, DMBA-treated. **C,** The average liver tumor numbers and the relative size distribution (classified as >6 mm, 2 mm–6 mm, ≤2 mm). **, $P < 0.01$. **D,** Macroscopic photograph of livers of male wild-type mice kept with ND (left), with ND and DCA 30 weeks (the second from left), with ND and DCA 55 weeks (the second from right), with HFD (right) for 30 weeks after the administration of DMBA. The arrowheads indicate HCCs. **E,** Immunofluorescence analysis of liver section. HSCs were visualized by α-smooth muscle actin staining (α-SMA; green) and the cell nuclei were stained by 4,6-diamidino-2-phenylindole (DAPI; blue). Arrowheads indicate α-SMA expressing cells that were positive for indicated markers (red). The histograms indicate the percentages of α-SMA expressing cells that were positive for indicated markers. Data of three to four individual mice in each group are represented as means ± SD. More than 100 cells in total were counted for statistical analysis. Data, means ± SD. *, $P < 0.05$; **, $P < 0.01$.

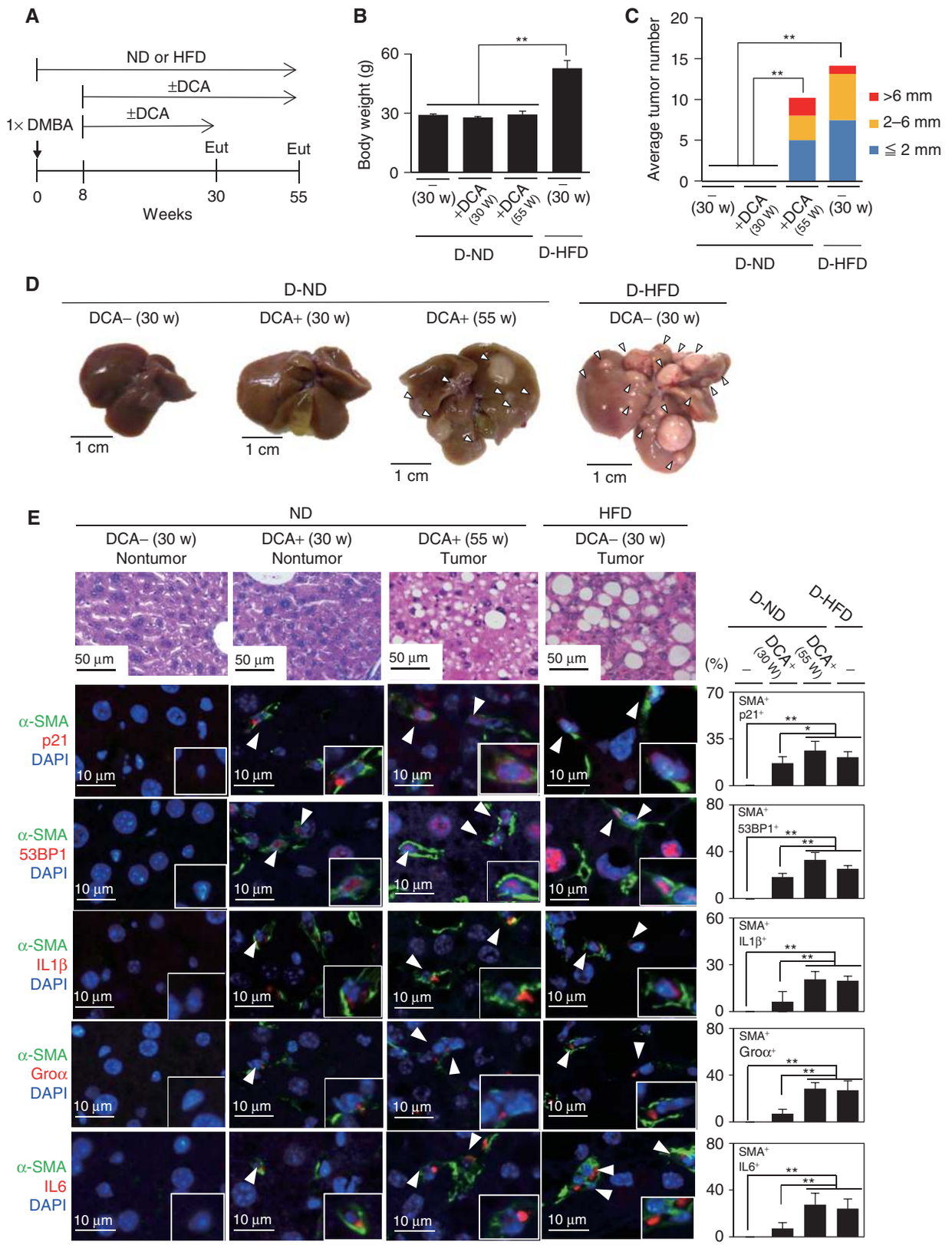

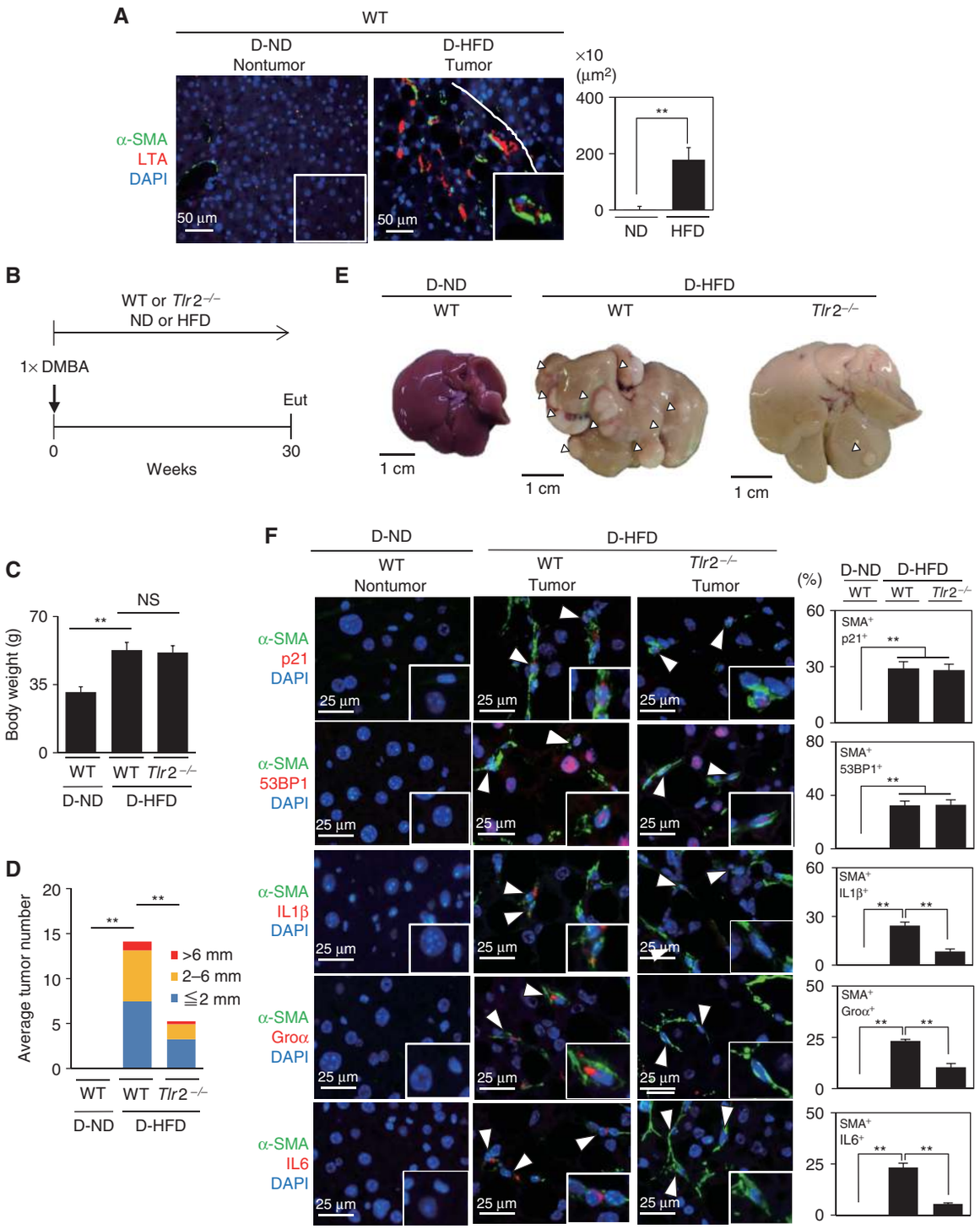

Figure 2. LTA and TLR2-mediated signaling promote obesity-associated HCC development. **A,** Immunohistochemical staining of LTA (red), α-SMA (green), and DAPI (blue) in 30-week-old male mouse liver sections. Scale bars, 50 μm. Data, means ± SD. **, $P < 0.01$. **B,** Timeline of the experimental procedure [wild-type (WT) ND, $n = 23$; WT HFD, $n = 15$; *Tlr2*$^{-/-}$, $n = 12$]. Eut, euthanasia; D, DMBA-treated. **C,** The average body weight of each group at the age of 30 weeks. Data, means ± SD. **, $P < 0.01$. D, DMBA-treated. **D,** The average liver tumor numbers and the relative size distribution (classified as >6 mm, 2 mm–6 mm, ≤2 mm). **, $P < 0.01$. **E,** Representative macroscopic photographs of liver. Arrowheads indicate HCCs. **F,** Immunofluorescence analysis of liver section. HSCs were visualized by α-smooth muscle actin staining (α-SMA; green) and the cell nuclei were stained by DAPI. Arrowheads indicate α-SMA expressing cells that were positive for indicated markers (red). The histograms indicate the percentages of α-SMA expressing cells that were positive for indicated markers. Scale bars, 25 μm. Data of three to four individual mice in each group are represented as means ± SD. More than 100 cells in total were counted for statistical analysis. Data, means ± SD. NS, not significant; **, $P < 0.01$.

DCA and LTA Cooperatively Induce the Expression of TLR2 and SASP Factors in Senescent HSCs

To investigate whether DCA and LTA cooperatively induce SASP factors in HSCs, primary HSCs isolated from mouse livers were treated with DCA for 8 days to prolong the senescent status and then stimulated with LTA (Fig. 3A). Consistent with our previous report (4), the expression of the senescence inducers p21 (encoded by *Cdkn1a*) and p16 (encoded by *Cdkn2a*) was upregulated by DCA treatment (Fig. 3B). Notably, the expression levels of TLR2 and SASP factors, such as IL1β, Groα, and IL6, were significantly enhanced by LTA in DCA-induced senescent HSCs (Fig. 3C). These responses by LTA were specifically mediated through TLR2 (Supplementary Fig. S3). Moreover, accumulation of LTA in the HFD-induced liver tumor area was well correlated with the percentage of senescent HSCs expressing SASP factors when examined using serial liver sections (Fig. 3D). These results suggest that LTA preferentially induced SASP factor production in DCA-induced senescent HSCs, and TLR2-mediated signals are enhanced by the upregulation of TLR2 itself by LTA. In addition, we observed the increased expression of the precancerous marker glypican 3 within hepatocytes in the livers of DCA- or DCA plus LTA–treated, ND-fed mice but not vehicle-treated mice (Supplementary Fig. S4). Moreover, the expression of tumor-promoting SASP factors, such as IL1β and Groα, was significantly enhanced in DCA plus LTA–treated mouse livers as compared with DCA- or vehicle-treated mice (Supplementary Fig. S4). In our previous study, we showed that vancomycin treatment significantly reduced obesity-associated liver cancer development (4). However, vancomycin treatment with DCA plus LTA significantly promoted liver cancer development, accompanied by increased levels of SASP factors (Supplementary Fig. S5). These results suggest that DCA and LTA have strong effects on liver carcinogenesis and could reverse the inhibitory effects of vancomycin on liver cancer development.

Prostaglandins Are Overproduced in HFD-Induced HCC

Next, we explored whether specific lipids were involved in obesity-associated HCC acceleration. Lipid accumulation is a hallmark of fatty liver and is involved in chronic liver diseases, including NAFLD, NASH, and HCC (29). Indeed, we observed severe lipid storage in the HFD-induced liver tumor area (Supplementary Fig. S6). Various studies have suggested that bioactive lipid mediators, such as omega-3 and omega-6 polyunsaturated fatty acids (PUFA), exhibited a variety of biological effects, including pro- or anti-inflammatory and procancer effects (30–32). Therefore, to analyze whether PUFAs were overproduced in HFD-induced liver tumors, liver tissues from DMBA-treated, HFD-fed mice were subjected to LC/MS-MS–based lipidomics analysis (31). High amounts of prostaglandins (PG), COX-mediated metabolites of arachidonic acid, were detected in liver tumor tissues as compared with the levels in nontumor areas (Supplementary Fig. S7A). In particular, TXB_2, PGD_2, PGE_2, and $PGF_{2\alpha}$ were abundant in the tumor region (Supplementary Fig. S7A). Interestingly, the levels of PGs in livers from vancomycin-treated, HFD-fed mice, where Gram-positive gut microbiota (phylum Firmicutes) are primarily targeted (Supplementary Fig. S7B), were significantly lower than those in livers from untreated mice (Supplementary Fig. S7A). These results suggest that PGs in the tumor areas are produced through a pathway where Gram-positive bacteria are involved.

We found that excess production of PGE_2 was detected in α-SMA–positive HSCs and that the frequency of PGE_2-producing HSCs was significantly decreased in the livers from TLR2-deficient mice or vancomycin-treated mice with decreased accumulation of LTA in the liver (Fig. 4A). COXs are rate-limiting enzymes involved in PG biosynthesis. The mRNA level of inducible *Cox2*, but not that of constitutive *Cox1*, was highly induced in the liver tumor tissues of wild-type mice (Fig. 4B). However, COX2 expression was significantly reduced in livers of TLR2-deficient or vancomycin-treated mice (Fig. 4A and B). Moreover, the level of PG inactivating enzyme 15-hydroxyprostaglandin dehydrogenase (15-PGDH) was significantly reduced in the liver tumor region, further facilitating the elevation of PG levels in the obesity-associated liver tumor region (Supplementary Fig. S7C and S7D). We found that COX2 was detected predominantly in the activated HSCs in the liver tumor region (Fig. 4A; Supplementary Fig. S7E), but at lower levels in $CD45^+$ or $F4/80^+$ immune cells (Supplementary Fig. S7E). The expression of COX2, but not COX1, in DCA-treated primary HSCs was significantly induced by increasing amounts of LTA (Fig. 4C), and the COX2 expression was dependent on TLR2 (Supplementary Fig. S3). Indeed, we confirmed that TLR2 was expressed in HSCs and this expression was enhanced by LTA alone or DCA plus LTA treatment (Supplementary Fig. S8A). On the other hand, hepatocytes did not express TLR2 (Supplementary Fig. S8B). Notably, phosphorylation of the inhibitor of κB (IκB), an indicator of the activation of NF-κB, was detected in HSCs in the liver tumor tissue from HFD-fed wild-type mice but not in HSCs from TLR2-deficient or vancomycin-treated mice (Fig. 4A). These results suggest that LTA may activate NF-κB through TLR2, and could induce the expression of SASP factors as well as COX2 to promote local production of PGs in DCA-induced senescent HSCs, thereby promoting HCC development in HFD-fed mice.

PGE_2 Suppresses Antitumor Immunity of the Host to Promote the HFD-Induced HCC Development

We next focused on determining which PG was most important for promoting obesity-associated HCC. Although PGs including PGE_2 have been shown to directly activate growth signals in epithelial cells of the gastrointestinal tract (33–35), we did not observe activation by PGs in hepatocytes (data not shown). On the other hand, because PGs have been reported to affect immune cells (36), we examined the effects of PGs on immune cells in the tumor microenvironment. We treated the immune cells isolated from liver tissues (Supplementary Fig. S8C) with PGs in the presence of LTA for 24 hours and measured cytokine production using a bead-based flow cytometric multiplex assay (Fig. 5A; Supplementary Fig. S8D and S8E). The production of IFNγ and TNFα, which are known to activate antitumor immune responses and inhibit cancer cell growth, was significantly and specifically

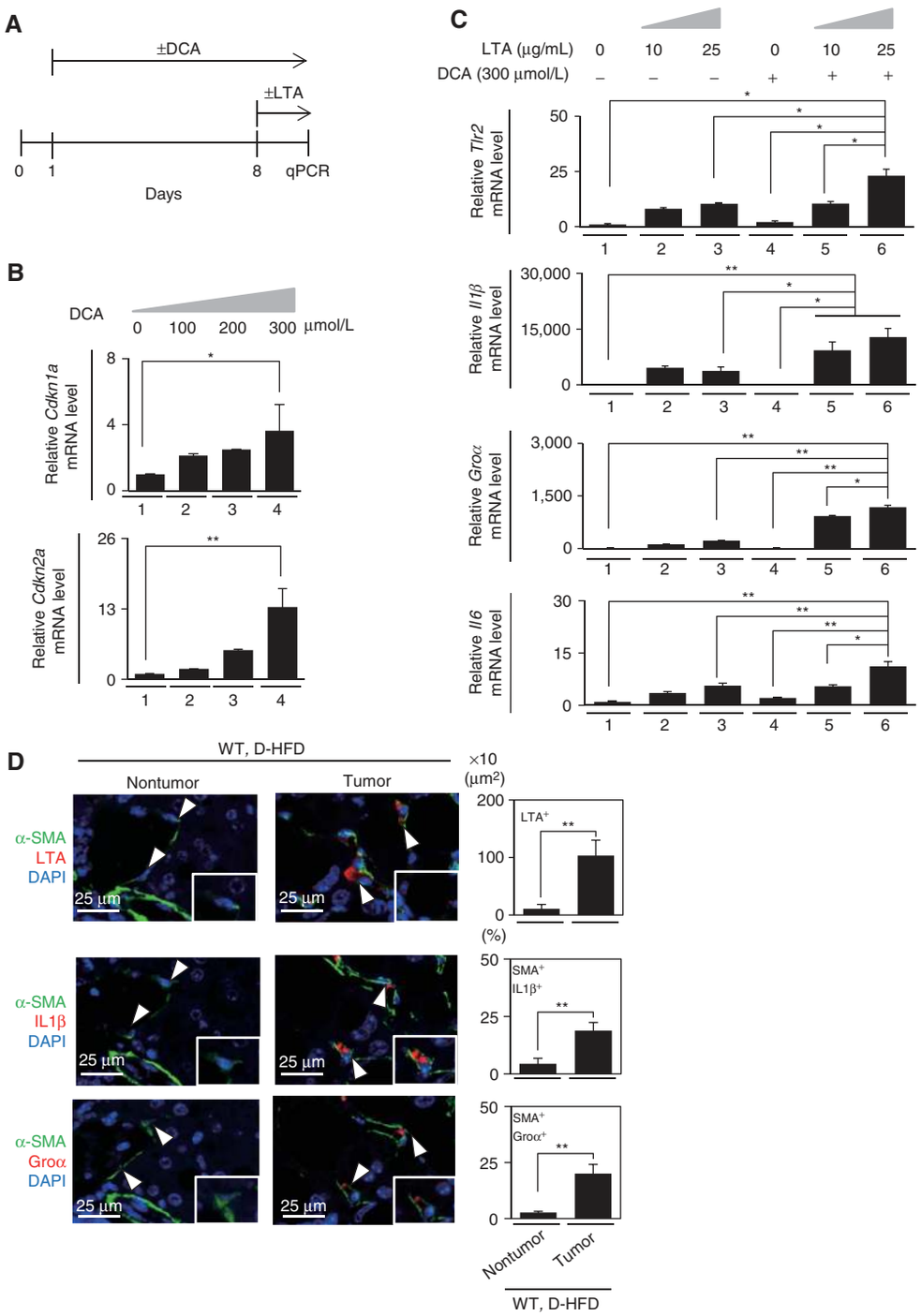

Figure 3. DCA and LTA cooperatively induce the expression of TLR2 and SASP factors in HSCs. **A,** Schematic representation of the experimental design. Murine primary HSCs were treated with medium containing DCA for 8 days to induce cellular senescence. Senescent HSCs were then incubated with LTA for 6 hours until collected. **B,** Murine primary HSCs were treated with medium containing DCA for 8 days to induce cellular senescence with following doses: lane 1 (0 mmol/L), lane 2 (100 mmol/L), lane 3 (200 mmol/L), and lane 4 (300 mmol/L). mRNA and cDNA were prepared from each sample and were subjected to RT-qPCR analysis for *Cdkn1a* (encoding p21) and *Cdkn2a* (encoding p16) gene expression. Data, means ± SD ($n = 3$). *, $P < 0.05$; **, $P < 0.01$. **C,** LTA was added to senescent murine primary HSCs as following doses: lane 1 (DCA, 0 mmol/L; LTA, 0 mg/mL), lane 2 (DCA, 0 mmol/L; LTA, 10 mg/mL), lane 3 (DCA, 0 mmol/L; LTA, 25 mg/mL), lane 4 (DCA, 300 mmol/L; LTA, 0 mg/mL), lane 5 (DCA, 300 mmol/L; LTA, 10 mg/mL), and lane 6 (DCA, 300 mmol/L; LTA, 25 mg/mL). mRNA and cDNA were prepared from each sample and were subjected to RT-qPCR analysis for *Tlr2*, *Il6*, *Groα*, or *Il1β* gene expression. Data, means ± SD. *, $P < 0.05$; **, $P < 0.01$. **D,** Immunofluorescence analysis of serial liver sections. HSCs were stained by α-SMA and cell nuclei were stained by DAPI. Arrowheads indicate α-SMA expressing cells that were positive for indicated markers. The histograms indicate the percentages of α-SMA expressing cells that were positive for indicated markers. Scale bars, 25 μm. Data of three to four individual mice in each group are represented as means ± SD. More than 100 cells in total were counted for statistical analysis. Data, means ± SD. *, $P < 0.05$; **, $P < 0.01$.

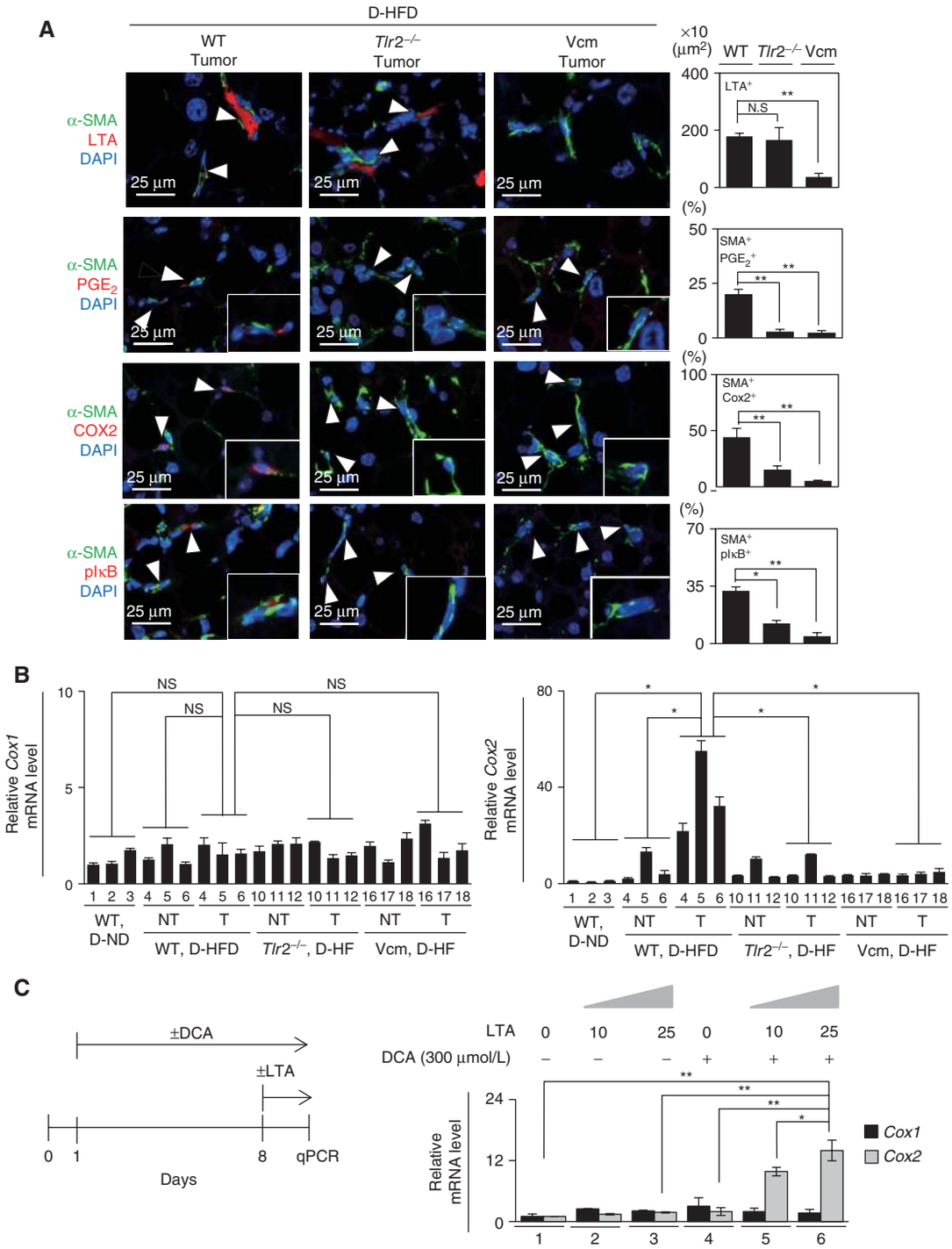

Figure 4. Prostaglandins, cyclooxygenase-mediated metabolites of arachidonic acid, are overproduced in the HFD-induced liver cancer. **A,** Immunofluorescence analysis of serial liver sections. HSCs were visualized by α-smooth muscle actin staining (α-SMA; green) and the cell nuclei were stained by DAPI. Arrowheads indicate α-SMA expressing cells that were positive for indicated markers (red). The histograms indicate the percentages of α-SMA–expressing cells that were positive for indicated markers. Scale bars, 25 μm. Number of mice analyzed, wild-type (WT), $n = 15$; *Tlr2*$^{-/-}$, $n = 12$; vancomycin (Vcm)-treated, $n = 9$. Data of three to four individual mice in each group are represented as means ± SD. More than 100 cells in total were counted for statistical analysis. Data, means ± SD. NS, not significant. *, $P < 0.05$; **, $P < 0.01$. D, DMBA-treated. **B,** The relative levels of *Cox1* or *Cox2* mRNA in non-tumor or tumor region of mice developed obesity-associated HCC analyzed by RT-qPCR. Representative results of three individual male mice are shown. Data of three individual mice are represented as means ± SD ($n = 3$). *, $P < 0.05$. **C,** LTA was added to senescent murine primary HSCs with following doses: lane 1 (DCA, 0 mmol/L; LTA, 0 mg/mL), lane 2 (DCA, 0 mmol/L; LTA, 10 mg/mL), lane 3 (DCA, 0 mmol/L; LTA, 25 mg/mL), lane 4 (DCA, 300 mmol/L; LTA, 0 mg/mL), lane 5 (DCA, 300 mmol/L; LTA, 10 mg/mL), and lane 6 (DCA, 300 mmol/L; LTA, 25 mg/mL). mRNA and cDNA were prepared from each sample and were subjected to RT-qPCR analysis for *Cox1* or *Cox2* gene expression. Data, means ± SD ($n = 3$). NS, not significant; *, $P < 0.05$; **, $P < 0.01$.

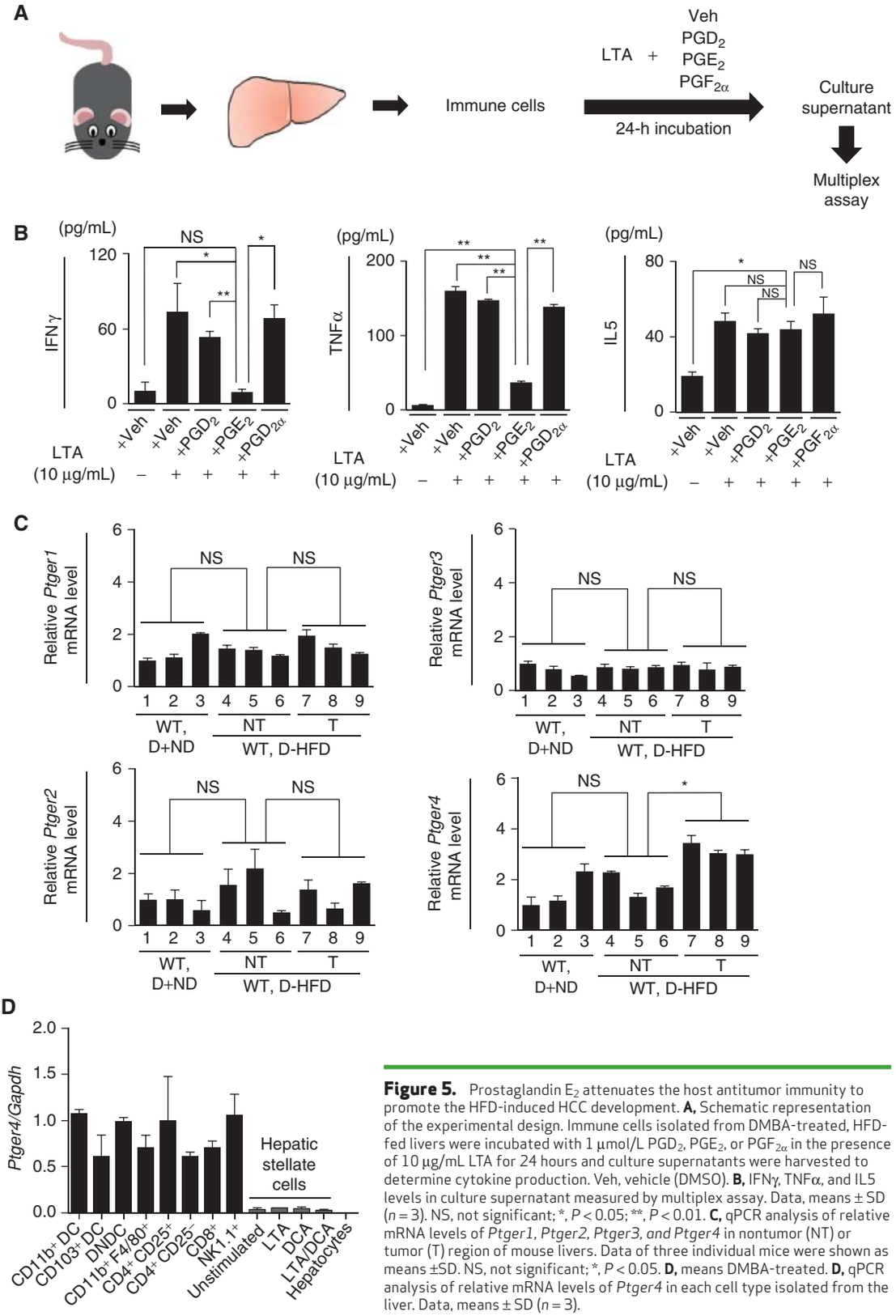

Figure 5. Prostaglandin E_2 attenuates the host antitumor immunity to promote the HFD-induced HCC development. **A,** Schematic representation of the experimental design. Immune cells isolated from DMBA-treated, HFD-fed livers were incubated with 1 μmol/L PGD_2, PGE_2, or $PGF_{2\alpha}$ in the presence of 10 μg/mL LTA for 24 hours and culture supernatants were harvested to determine cytokine production. Veh, vehicle (DMSO). **B,** IFNγ, TNFα, and IL5 levels in culture supernatant measured by multiplex assay. Data, means ± SD ($n = 3$). NS, not significant; *, $P < 0.05$; **, $P < 0.01$. **C,** qPCR analysis of relative mRNA levels of *Ptger1, Ptger2, Ptger3, and Ptger4* in nontumor (NT) or tumor (T) region of mouse livers. Data of three individual mice were shown as means ±SD. NS, not significant; *, $P < 0.05$. **D,** means DMBA-treated. **D,** qPCR analysis of relative mRNA levels of *Ptger4* in each cell type isolated from the liver. Data, means ± SD ($n = 3$).

attenuated by PGE_2 (Fig. 5B). In contrast, the production of IL10, a potent anti-inflammatory cytokine, and IL6, a known tumor-promoting cytokine, in immune cells was slightly but significantly enhanced (Supplementary Fig. S8D). The production of IL5, a Th2 cytokine, was unchanged in the presence of any PGs, and other cytokines (IL2, IL4, IL9, IL13, IL17A, IL17F, IL21, and IL22) were undetectable (Fig. 5B and data not shown). We confirmed that TLR2, which recognizes LTA, was expressed on many types of immune cells, such as DCs, macrophages, and granulocytes, but not on T cells isolated from the HFD-treated liver (Supplementary Fig. S8E). These results suggest that PGE_2 could strongly attenuate antitumor immune responses.

A PTGER4 Antagonist Inhibits the Growth of HFD-Induced HCC

PGE_2 is known to be recognized by four types of receptors: PTGER1, PTGER2, PTGER3, and PTGER4 (37, 38). In our mouse model, the expression of PTGER4, but not other PGE_2 receptors, was significantly upregulated in tumor tissues (Fig. 5C), suggesting that PTGER4 could predominantly mediate PGE_2 signaling in HFD-induced liver tumor tissue. We confirmed that PTGER4 receptors were expressed only on immune cells we examined but not on hepatocytes or HSCs (Fig. 5D), suggesting that PGE_2 produced by senescent HSCs, which express TLR2 but not PTGER4, continuously affects immune cells, particularly on T cells, which express PTGER4 but not TLR2 (Fig. 5D; Supplementary Fig. S8A, B, and E).

To clarify the importance of PGE_2 and its receptor PTGER4, we used the PTGER4-specific antagonist AAT-008, 4-[(1S)-1-({[5-chloro-2-(3-fluorophenoxy) pyridin-3-yl]carbonyl}amino) ethyl] benzoic acid. Mice were treated with this PTGER4 antagonist every day from 19 weeks of age to 30 weeks of age (Fig. 6A). Interestingly, HCC development in AAT-008–treated mice was strongly attenuated compared with vehicle-treated mice (Fig. 6B and D). Notably, however, AAT-008 treatment did not influence body weight (Fig. 6C).

Next, we assessed the impact of PTGER4 blockade on the prevalence and activation status of immune cells. Although the frequencies of $CD11c^{hi}$ MHC class II^{hi} dendritic cells (DC) and $CD11b^+$ DCs were not changed, the population of $CD103^+$ DCs, which are essential for anticancer immune responses (39, 40), was increased in the AAT-008–treated group (Fig. 6E; Supplementary Fig. S9A). The frequency of $CD4^+FOXP3^+$ regulatory T cells (Treg), but not $CD4^+FOXP3^-$ T cells, was significantly reduced by AAT-008 treatment (Fig. 6F; Supplementary Fig. S9B). In addition, the ratio of $CD8^+$ T cells to Tregs was increased in AAT-008–treated mice, although the frequency of $CD8^+$ T cells was not changed (Fig. 6F). Moreover, the number of $CD8^+$ T cells expressing the activation marker CD69 was significantly increased in livers from AAT-008–treated mice (Fig. 6F; Supplementary Fig. S9C). In contrast, administration of AAT-008 significantly reduced the number of $CD8^+$ T cells expressing programmed cell death-1 (PD-1), a key inhibitory receptor on T cells in the tumor microenvironment (Fig. 6F; Supplementary Fig. S9D). These results suggest that blockade of the PTGER4 pathway could reactivate antitumor immunity in the obesity-associated liver tumor microenvironment.

COX2 Overexpression and Excess PGE_2 Production Are Detected in Noncirrhotic NASH-Associated HCC in Humans

Finally, we sought to determine whether PGE_2 was indeed a biomarker mediating the development of NASH-associated HCC in humans. Approximately 20% of NASH-associated HCC is nonfibrotic and arises directly from NAFLD-based NASH (41, 42), and this is categorized as noncirrhotic NASH-associated HCC. We previously found that the histology of HFD-induced HCC in our mouse model is less fibrotic and that this mouse model could be used as an animal model for noncirrhotic NASH-associated HCC in humans (4). Therefore, we histologically classified NASH-associated HCC into four groups: (i) HCCs with low lipid accumulation in fibrotic NASH, (ii) HCCs with high lipid accumulation in fibrotic NASH, (iii) HCCs with low lipid accumulation in nonfibrotic NASH, and (iv) HCCs with high lipid accumulation in nonfibrotic NASH (Supplementary Fig. S10). Interestingly, COX2 expression was predominantly detected in senescent HSCs in the HCCs with high lipid accumulation arising from nonfibrotic NASH, whereas lower COX2 expression was observed in other three groups (Fig. 7A). The SASP factor expression and the excess PGE_2 biosynthesis was observed in the COX2-expressing HSCs in HCCs with high lipid accumulation in nonfibrotic NASH (Fig. 7A). These results suggest a similar mechanism could occur in human NASH-associated HCCs, and high COX2 expression and PGE_2 overproduction were observed specifically in HCCs with high lipid accumulation in nonfibrotic NASH.

DISCUSSION

HCC is the second leading cause of cancer mortality worldwide (43). Although long-term infection with HBV or HCV is a well-known risk factor for HCC, obesity-associated NAFLD and NASH have recently emerged as important causes of HCC (6). Owing to the increased incidence of obesity-associated HCC (42), the mechanisms involved in this disease have been extensively investigated. Previous reports have suggested that endoplasmic reticulum stress, p62/SQSTM accumulation, and increased mitochondrial ROS levels in hepatocytes are important causes of hepatocyte carcinogenesis (3). Although these reports have focused on the initial onset of liver carcinogenesis (44), the progression mechanisms of obesity-associated liver cancer are still incompletely understood, particularly in the context of the gut–liver axis.

In this study, we showed that the gut–liver axis plays important role in obesity-associated liver cancer development. The hepatic translocation of DCA, an obesity-induced Gram-positive gut microbial metabolite, promoted cellular senescence in HSCs. The Gram-positive gut microbiota also provided its component LTA to the liver to synergistically induce the expression of SASP factors and the innate immune receptor TLR2 in DCA-induced senescent HSCs. Furthermore, LTA upregulated COX2 expression in the senescent HSCs to promote local production of PGs. In particular, PGE_2 was likely to suppress the antitumor immune response through the PTGER4 receptor on immune cells, and we found that an PTGER4 antagonist significantly suppressed obesity-induced HCC development with the reactivation of antitumor immunity (Fig. 7B).

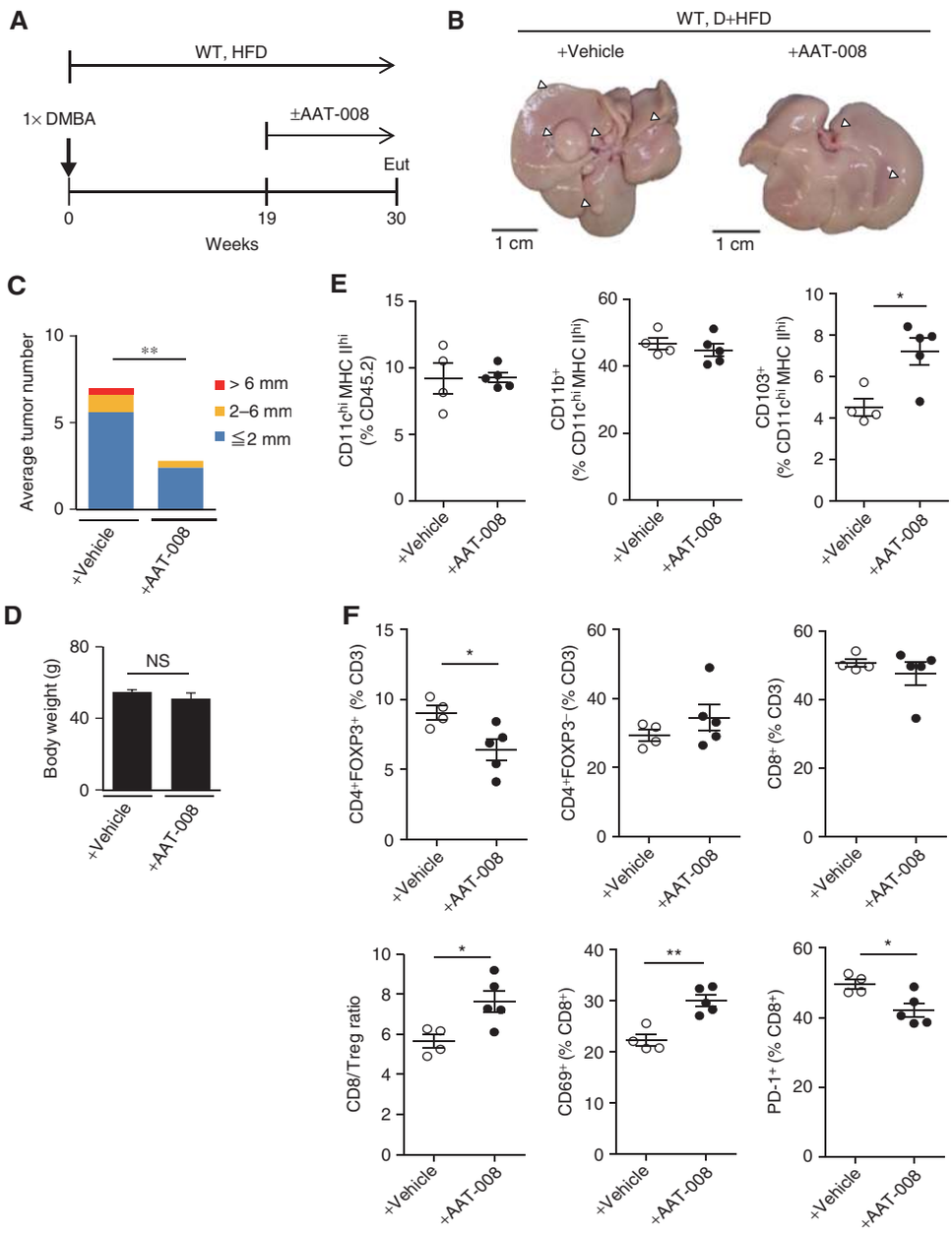

Figure 6. PTGER4 antagonist attenuates the HFD-induced HCC development. **A,** Timeline of the experimental procedure (vehicle, $n = 5$; PTGER4 antagonist, $n = 5$). Eut, euthanasia. **B,** Representative macroscopic photographs of liver. Arrowheads indicate HCCs. **C,** The average liver tumor numbers and the relative size distribution (classified as >6 mm, 2 mm–6 mm, ≤2 mm). **, $P < 0.01$. **D,** The average body weight of each group at the age of 30 weeks. Data, means ± SD. **E,** Flow cytometry analysis of immune cells between vehicle- and PTGER4 antagonist–treated mice. The percentages of total $CD11c^{hi}$ MHC class II^{hi} ($MHC\ II^{hi}$), $CD11b^{+}$ $CD11c^{hi}$ MHC II^{hi}, or $CD103^{+}$ $CD11c^{hi}$ MHC II^{hi} cells were analyzed by flow cytometry. Data, means ± SEM. ($n = 4$–5, the number of dots reflects mouse number). **F,** The percentages of $CD3^{+}$ $CD4^{+}$ $FOXP3^{+}$, $CD3^{+}$ $CD4^{+}$ $FOXP3^{-}$, $CD3^{+}$ $CD8^{+}$, $CD69^{+}$ $CD8^{+}$, or $PD\text{-}1^{+}$ $CD8^{+}$ cells were analyzed by flow cytometry. The ratio of $CD8^{+}$ T cells to $CD4^{+}$ $FOXP3^{+}$ Tregs was calculated. Data, means ± SEM. ($n = 4$–5, the number of dots reflects mouse number); NS, not significant, *, $P < 0.05$; **, $P < 0.01$.

Recent studies have provided insight into the effects of the gut–liver axis in some liver diseases, such as fatty liver, hepatitis, liver fibrosis, and HCC with fibrosis (4, 28, 45); these effects are thought to be mediated by absorption of intestinal contents, including gut microbiota–related metabolites and components, which directly affect liver homeostasis (46). The gut microbiota not only alters the form of metabolites to be absorbed, but also supplies ligands for the activation of innate immunity, which could stimulate proinflammatory responses in the liver (46). Other groups have reported that LPS, a cell surface component of the Gram-negative gut microbiota, promotes liver fibrosis and fibrotic liver cancer

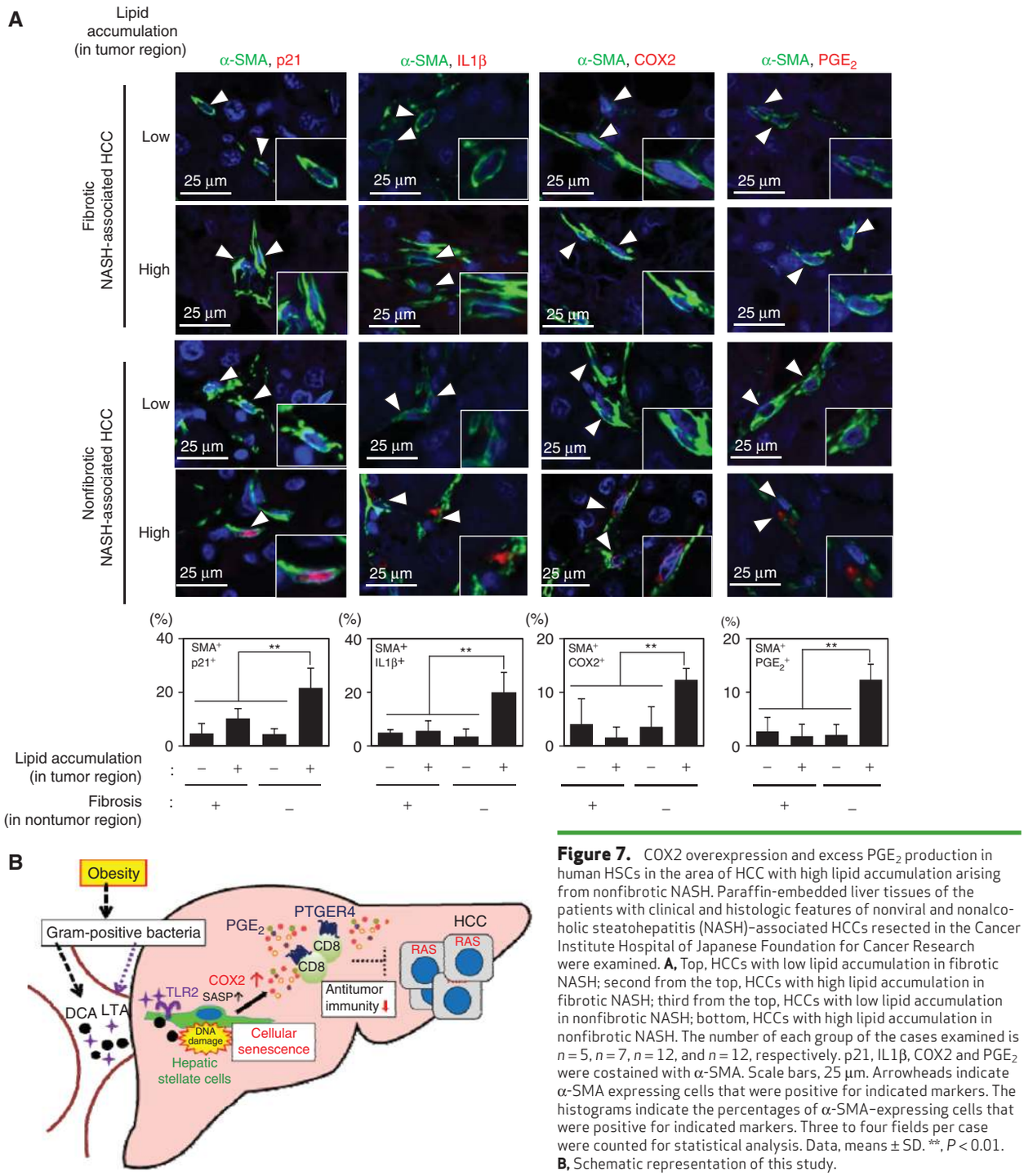

Figure 7. COX2 overexpression and excess PGE_2 production in human HSCs in the area of HCC with high lipid accumulation arising from nonfibrotic NASH. Paraffin-embedded liver tissues of the patients with clinical and histologic features of nonviral and nonalcoholic steatohepatitis (NASH)–associated HCCs resected in the Cancer Institute Hospital of Japanese Foundation for Cancer Research were examined. **A,** Top, HCCs with low lipid accumulation in fibrotic NASH; second from the top, HCCs with high lipid accumulation in fibrotic NASH; third from the top, HCCs with low lipid accumulation in nonfibrotic NASH; bottom, HCCs with high lipid accumulation in nonfibrotic NASH. The number of each group of the cases examined is $n = 5$, $n = 7$, $n = 12$, and $n = 12$, respectively. p21, IL1β, COX2 and PGE_2 were costained with α-SMA. Scale bars, 25 μm. Arrowheads indicate α-SMA expressing cells that were positive for indicated markers. The histograms indicate the percentages of α-SMA–expressing cells that were positive for indicated markers. Three to four fields per case were counted for statistical analysis. Data, means ± SD. **, $P < 0.01$. **B,** Schematic representation of this study.

in mice (26). In this study, we clarified that DCA and LTA derived from the obesity-induced Gram-positive gut microbiota cooperated to upregulate the expression of SASP factors and COX2 in DCA-induced senescent HSCs, suggesting a unique role of the gut microbiota in the development of obesity-associated HCC.

Our results also suggested the importance of excess biosynthesis of PGE_2 through the COX2 pathway in a TLR2-dependent manner in obesity-associated liver carcinogenesis. PGE_2 production was confirmed in the senescent HSCs, suggesting that senescence-associated lipid mediators also play pivotal roles with other SASP factors in the tumor-promoting microenvironment. This COX2-mediated product, PGE_2, is known to be a key factor in cancer progression through directly activating Wnt signals (33–35). Moreover, PGs are known to affect immune cells (29). Indeed, in our study,

among the COX2-mediated products examined, PGE_2 was likely to be the primary contributor to the progression of obesity-induced HCC by inhibiting antitumor cytokine production from liver immune cells. PGE_2 is known to function through four receptors, i.e., PTGER1, PTGER2, PTGER3, and PTGER4, a family of G protein–coupled receptors (37, 38). In the present study, we confirmed that PTGER4 expression was significantly upregulated in immune cells, whereas those of other three receptors were not upregulated, in obesity-associated liver tumor tissues. Furthermore, treatment with a PTGER4 antagonist strongly inhibited obesity-associated liver tumor development by reactivating antitumor immunity, indicating that the PTGER4 receptor played a significant role in mediating the effects of PGE_2 in our obesity-associated HCC model.

Using tissues of human patients with nonfibrotic NASH-associated HCC with high levels of lipid accumulation in the tumor region, we observed that COX2 was overexpressed, with the concomitant detection of excess PGE_2 production in the senescent HSCs, consistent with the findings in our mouse model. In previous reports, approximately 20% of NASH-associated HCC was found to be nonfibrotic and to have arisen directly from NAFLD-based NASH (41, 42); this was categorized as noncirrhotic NASH-associated HCC. We previously demonstrated that our mouse model developed histologically less fibrotic and lipid-accumulated HCCs, representing a potent novel animal model for human noncirrhotic NASH-associated HCCs (4). Our current results further identified that COX2 upregulation and PGE_2 overproduction were preferentially detected in HCCs with high lipid accumulation in nonfibrotic NASH. These results, therefore, suggested that PGE_2 could similarly function in human NASH-associated HCC and implied that this PGE_2-associated pathway may have applications as a therapeutic target for nonfibrotic NASH-associated liver cancer. However, further studies are needed to identify the involvement of the PGE_2 receptor in these pathways in humans.

Increasing evidence has suggested that the PGE_2/PTGER4 pathway is important for immunosuppression (37, 38). $CD103^+$ DCs are a subpopulation of DCs that are indispensable for antitumor immunity owing to their role in the activation of $CD8^+$ T cells (39). We found that $CD103^+$ DCs, but not $CD103^-$ $CD11b^+$ DCs, were increased in liver tissues following treatment with the PTGER4 antagonist AAT-008. We further showed that inhibition of the PTGER4 pathway significantly reduced the numbers of Tregs and PD-1^+ $CD8^+$ T cells. Tregs can potently inhibit antitumor T-cell responses and can induce the expression of inhibitory molecules, such as PD-1, on $CD8^+$ T cells (47). PD-1 signaling impairs T-cell responses, including IFNγ and TNFα production, and PD-1^+ $CD8^+$ T cells are present in the context of functional impairment. The PD-1 blockade can recover the functions of effector T cells, and an anti–PD-1 antibody is now being clinically used for the treatment of various cancers (48, 49). Interestingly, we also found that production of IFNγ and TNFα by LTA-stimulated liver immune cells was suppressed by PGE_2. These observations suggested that PGE_2 may impair the antitumor functions of $CD8^+$ T cells by inhibiting $CD103^+$ dendritic cell accumulation and enhancing Treg prevalence in obesity-associated HCC, although further studies are needed to determine which cells directly respond to LTA and PGE_2.

In summary, we identified the collaborative role of DCA and LTA derived from Gram-positive gut microbiota in the induction of SASP factors and COX2 expression through TLR2-mediated signaling in senescent HSCs in obesity-associated liver tumors. COX2-mediated production of PGE_2 was found to facilitate tumor progression through suppression of antitumor immunity. These findings indicated that lipid mediators, such as PGs, are also produced in senescent cells and function as SASP factors. Additionally, our data suggested that PTGER4 antagonists may represent novel therapeutic drugs for obesity-associated HCC, particularly in the context of combination therapy with anti–PD-1 antibodies, because PTGER4 antagonist treatment significantly reduced the ratio of PD-1–expressing $CD8^+$ T cells in our setting. These findings provide valuable new insights into the regulation of the tumor microenvironment and the development of potent anticancer drugs, and may facilitate the prevention and treatment of obesity-associated liver cancer, although further studies are needed to identify the functioning PGE_2 receptor in human noncirrhotic NASH-associated HCC.

METHODS

Mice and Diet

C57/BL6 mice were purchased from CLEA Japan Inc. The *Tlr2*$^{-/-}$ mice (C57/BL6) were purchased from Oriental Yeast Co. Ltd. Male mice were used for all the experiments in this study. The mice were maintained under specific pathogen-free conditions, on a 12-hour light–dark cycle, and fed a normal diet (Labo MR) or high-fat diet (D12492, Research Diet Inc.) *ad libitum*. Mice weighing more than 45 g at 30 weeks old were used as obese mice for all experiments. The sample size used in this study was determined based on the expense of data collection and the need to have sufficient statistical power. Randomization and blinding were not used in this study. All animal experiments followed protocols approved by the Animal Care and Use Committee of Tokyo University of Science (Tokyo, Japan).

Chemically Induced Carcinogenesis

DMBA (Sigma) treatments were performed as described previously (4). In brief, 50 μL of a solution of 0.5% DMBA (Sigma) in acetone was applied to the dorsal surface of mice on postnatal days 4 to 5. After this application, mother mice with pups were fed ND or HFD. At the age of 4 weeks old, pups were weaned and continuously fed either ND or HFD until euthanized. Evaluation of tumor number and size was determined by counting the number of visible tumors and measuring the size of the tumor.

Treatment of Deoxycholic Acid and Antibiotics In Vivo

DCA (Wako) was dissolved in absolute ethanol and diluted in 66% propylene glycol (Wako) to reduce the concentration of alcohol to 5%. Mice treated with DMBA at neonatal stage were fed with ND supplemented with 0.3% DCA or vehicle-supplemented ND (control) at the age of 8 weeks old until euthanized. ND-fed mice treated with DMBA at neonatal stage were intraperitoneally treated with 200 μL of a solution of 5 mg/mL LTA (Sigma, L2515) or water (vehicle) every day at the age of 22 weeks old until euthanized. HFD-fed mice

treated with DMBA at neonatal stage were treated with vancomycin (500 mg/L) in drinking water. HFD-fed mice treated with DMBA at neonatal stage were administered with 40 μg per g (weight) of DCA or vehicle three times per week using a plastic feeding tube and treated with 200 μL of a solution of 5 mg/mL LTA or vehicle every day. The administration schedules of vancomycin, DCA, and LTA in HFD-fed mice are described in each figure legend.

Treatment with PTGER4 Antagonist

A PTGER4 receptor specific antagonist, AAT-008, was kindly provided by AskAt Inc. AAT-008 is 4-[(1S)-1-({[5-chloro-2-(3- fluorophenoxy) pyridin-3-yl]carbonyl}amino)ethyl] benzoic acid (Ki = 0.97 nmol/L for human PTGER4), and its activity against human, mouse, and rat PTGER4 receptors was examined and proven equivalent (49). AAT-008 was dissolved in 0.5% methylcellulose solution, and HFD-fed mice treated with DMBA at the neonatal stage were orally administered AAT-008 (30 mg/kg) or vehicle everyday using a feeding tube, at the age of 19 weeks old until euthanized.

Histology and Immunofluorescence Analysis

Hematoxylin and eosin staining and immunofluorescence analysis were performed as previously described (4). The primary antibodies for mouse samples were as follows: α-SMA (Sigma A5228, mouse monoclonal), α-SMA (Abcam, ab5964, rabbit polyclonal), p21 (Abcam, ab2961), 53BP1 (Santa Cruz, sc22760), IL6 (Abcam ab6672), Groα (Abcam, ab17882), IL1β (R&D Systems, AF-401-NA), F4/80 (Invitrogen, BM8), CD45 (Millipore, 05-1416), LTA (Lifespan Biosciences, LS-C202488), PGE_2 (Abcam, ab2318), COX2 (Abcam, ab15191), Glypican 3 (Abcam, ab66596), and phospho-IκB (Cell Signaling Technology, 9246). The primary antibodies for human samples were as follows: α-SMA (Dako, M0851), COX2 (Abcam, ab15191), and PGE_2 (Abcam, ab2318). PGE_2 staining was performed as previously reported (50).

Oil Red O Staining

Frozen sections (5-μm-thick) of livers were washed in 60% isopropanol and were incubated with six parts oil red O solution (0.3 g oil red O in 100 mL isopropanol) and 4 parts H_2O for 13 minutes at 37°C. After washing in 60% isopropanol and tap water, the sections were counterstained with hematoxylin.

Western Blot Analysis

Tissue lysates were prepared using a homogenizer in lysis buffer (50 mmol/L HEPES (pH7.5), 150 mmol/L NaCl, 1 mmol/L EDTA, 2.5 mmol/L EGTA, 10% glycerol, 0.1% Tween 20, and 10 mmol/L β-glycerophosphate) containing protease inhibitor cocktail (Nacalai Tesque). The transferred membranes were immunoblotted directly with antibodies, and the signals were detected using an enhanced chemiluminescence system (GE Healthcare). The first antibodies used were as follows: 15-PGDH/HPGD (Novus Biologic, NB200-179) and GAPDH (Abcam, ab9485).

Bacterial 16S rRNA Amplicon Sequencing and Analysis

Bacterial genomic DNA was isolated from feces using a QIAamp DNA Stool mini kit (QIAGEN), following the manufacturer's instructions. DNA from fecal samples was amplified using the universal 16S rRNA primers F515 5′-GTGCCAGCMGCCGCGGTAA-3′ and R806 5′-GGACTACHVGGGTWTCTAAT-3′ targeting the V4 hyper variable region of the 16S rRNA gene using KOD FX DNA polymerase (TOYOBO). 16S rRNA libraries for all samples were prepared and sequenced by Illumina MiSeq platform, following the manufacturer's instructions, Preparing 16S Ribosomal RNA Gene Amplicons for the Illumina MiSeq System. All samples were paired-end sequenced with 180-bp read length to a targeted sequencing depth of 7.5G bp. All reads that had any ambiguous base calls and average quality score below 25 were removed using custom Perl script. The preanalyzed reads having at least 97% identity were subjected to OTU analysis and removed putative chimeric reads using UCLUST and UCHIME. Representative sequences from each OTU were blasted to the database in Ribosomal Database Project (RDP) and aligned by the RDP Classifier. The obtained OTU sequences were grouped at the phylum level.

Mediator Lipidomics

LC/MS-MS–based lipidomics analyses were performed using a high-performance liquid chromatography system (Waters UPLC) with a linear ion-trap quadrupole mass spectrometer (QTRAP5500; AB SCIEX) equipped with an Acquity UPLC BEH C_{18} column (Waters) as described previously (30). MS-MS analyses were conducted in negative-ion mode, and fatty-acid metabolites were identified and quantified by multiple reaction monitoring.

Primary Cell Culture

Murine primary hepatic stellate cells were isolated by the following procedure. Briefly, the livers were isolated from the blood-removed 10-week-old mice. The gall bladder was removed, and then the livers were carefully excised into small pieces. The small liver pieces were incubated in PBS containing 0.05% trypsin and 0.53 mmol/L EDTA (Nacalai Tesque) for 14 minutes at 37°C with gentle mixing at every 2 minutes. The cells were passed through 70-μm cell strainers (BD Biosciences), washed with DMEM supplemented with 10% FBS at least two times, and cultured in tissue culture dishes. After five days, α-SMA–positive cells were confirmed by cell staining and quantitative PCR analysis, and used as active hepatic stellate cells. The murine primary HSCs were cultured in the absence or presence of DCA (100, 200, or 300 μmol/L) for 8 days, and then were treated with LTA (10 or 25 μg/mL, Invivogen) for 6 hours until harvested. Primary hepatocytes were collected using the following methods. The mouse livers were perfused slowly via the inferior vena cava with 30 mL of warm liver perfusion medium [33 mmol/L glucose, 100 mmol/L NaCl, 2.3 mmol/L KCl, 1.2 mmol/L KH_2PO_4, 25 mmol/L HEPES, 1.5% FBS, 1% GlutaMAX supplement (Gibco), and 0.5 mmol/L EGTA] at a rate of 5 mL/min, and then digested with 40 mL of liver digest medium (liver perfusion buffer containing 6.5 mmol/L $CaCl_2$ and 50 μg/mL Liberase TM) at a rate of 5 mL/minute. After the gall bladder was removed, the livers were carefully excised and incubated in liver digest medium for 5 min at 37°C, and passed through a 100-μm cell strainer (BD Biosciences). Hepatocytes were collected by centrifuging the cell suspension at 50 × g for 2 minutes and used for flow cytometric analysis. The collected hepatocytes were also confirmed by their morphology and hepatocyte marker expression by quantitative PCR analysis, and used as hepatocytes. These primary murine cells were prepared every time for each experiment and were not passaged. Therefore, they were not authenticated for their clonality. These cells were tested each time by PCR-based assay to verify that they were free of *Mycoplasma* contamination.

Quantitative PCR

Total RNA was extracted from mouse tissues or cultured cells using TRIzol reagent (Life Technologies) and reverse transcription and quantitative PCR were performed as previously described (23). Primers used were as follows: mouse *Gapdh,* 5′-CAACTACATGGTCTACATGTTC-3′ (forward) and 5′-CACCAGTAGACTCCACGAC-3′ (reverse); mouse *Cdkn1a*,5′-GTGATTGCGATGCGCTCATG-3′(forward)and5′-TCTCTTGCAGAAGACCAATC-3′ (reverse); mouse *Cdkn2a*, 5′-AGGGCCGTGTGCATGACGTG-3′ (forward) and 5′-GCACCGGGCGGGAGAAGGTA-3′ (reverse); mouse *Il1β*, 5′-GGACCCATATGAGCTGAAAGCT-3′ (forward) and 5′-TGTCGTTGCTTGGTTCTCCTT-3′ (reverse); mouse *Il6*, 5′-AGAAGGAGTGGCTAAGGACCAA-3′ (forward) and 5′-AACG

CACTAGGTTTGCCGAGTA-3′ (reverse); mouse *Groα*, 5′-GCTGG GATTCACCTCAAGAA-3′ (forward) and 5′-AGGTGCCATCAGAGCAG TCT-3′ (reverse); mouse *Tlr2*, 5′-TGGAGCATCCGAATTGCATCACCG-3′ (forward) and 5′-GGCCACCAAGATCCAGAAGAGCC-3′ (reverse); mouse *Cox1*, 5′-GTGCTGGGGCAGTGCTGGAG-3′ (forward) and 5′-TGGGG CCTGAGTAGCCCGTG-3′ (reverse); mouse *Cox2*, 5′-AACCGCATTGC CTCTGAAT-3′ (forward) and 5′-CATGTTCCAGGAGGATGGAG-3′ (reverse); mouse *Ptger1*, 5′-GGGATGCTCGAAACACCAGA-3′ (forward) and 5′-TTGGGGTTTTAAGGCCGTGT-3′ (reverse); mouse *Ptger2*, 5′-CTCCAAGCTAATGGAGGACTG-3′ (forward) and 5′-GATAAGTGG CGCCTGTAGAAG-3′ (reverse); mouse *Ptger3*, 5′-TGTCGGTTGAGCAA TGCAAGACAC-3′ (forward) and 5′-TCTGGCAGAACTTCCGAAG AAGGA-3′ (reverse); mouse *Ptger4*, 5′-TACTTCTACAGCCACTACGT GGAC-3′ (forward) and 5′-TGGTCCAGTCGATGAAGCACCAGG-3′ (reverse); mouse *15-PGDH*, 5′-ACGGCATCATCGGATTCACA-3′ (forward) and 5′-CAAAGCCTGGGCAAATGACA-3′ (reverse); Firmicutes 16S rRNA, 5′-GGAGYATGTGGTTTAATTCGAAGCA-3′ (forward) and 5′-AGCTGACGACAACCATGCAC-3′ (reverse).

Immune Cell Isolation, Stimulation, and Multiplex Bead-Based Assay

Livers obtained from mice were minced with scissors and incubated in PBS (supplemented with 5% fetal bovine serum, 0.1 μg/mL $CaCl_2$, and 0.1 μg/mL $MgCl_2$) containing 61.5 μg/mL Liberase TM (Roche) and 10 μg/mL DNase I (Roche) for 30 minutes at 37°C. Digested tissues were further incubated for 5 minutes in the presence of 5 mmol/L EDTA (Dojindo Laboratories) and passed through a 100-μm cell strainer (BD Biosciences). Red blood cells were lysed by RBC lysis buffer (BioLegend), and the cells were filtered through a 70-μm cell strainer (BD Biosciences). The cells were cultured in the presence of 1 μmol/L PGD_2, PGE_2, or $PGF_{2\alpha}$ (Cayman Chemical) with or without 10 μg/mL LTA (Invivogen) for 24 hours. Supernatants were assayed for cytokines by multiplex assay using the LEGENDplex Mouse Th Cytokine Panel (13-plex; BioLegend), according to the manufacturer's instructions.

Flow Cytometry

Cells were preincubated with unlabeled anti-CD16/32 mAb (2.4G2; TONBO) to avoid nonspecific binding of antibodies to FcγR. Cells were then incubated with the antibodies for CD3ε (145-2C11), CD4 (RM4-5), CD8α (53-6.7), CD11b (M1/70), CD11c (N418), CD45.2 (104), CD69 (H1.2F3), CD103 (2E7), I-A/I-E (M5/114.15.2), KLRG1 (2F1/KLRG1), NK1.1 (PK136; all from BioLegend), PD-1 (J43; BD Biosciences), and TLR2 (T2.5; eBioscience). Cells were fixed and permeabilized using a FOXP3 staining buffer kit (eBioscience), and then intracellularly stained for FOXP3 (FJK-16s; eBioscience). Murine primary HSCs and freshly isolated hepatocytes were preincubated with unlabeled anti-CD16/32 mAb (2.4G2), and then incubated with the antibody for TLR2 (T2.5). Stained cells were analyzed by Attune NxT (Life Technologies) and data were processed by FlowJo Version 10 software (FlowJo). Dead cells were excluded by using Zombie NIR fixable viability dye (BioLegend).

Quantification of Ptger4 *mRNA Levels*

$CD11b^+$ DCs ($CD11b^+CD103^-CD11c^{hi}$MHC class II^{hi}), $CD103^+$ DCs ($CD11b^-CD103^+CD11c^{hi}$MHC class II^{hi}), double-negative DCs ($CD11b^-CD103^-CD11c^{hi}$MHC class II^{hi}), $CD11b^+F4/80^+$ macrophages, $CD4^+CD25^+$ Tregs, $CD4^+CD25^-$ T cells, $CD8^+$ cells, and $NK1.1^+$ cells were sorted from mouse livers by FACS Aria II cell sorter (BD Biosciences). Total RNA was extracted using a RNeasy Plus Micro kit (QIAGEN) according to the manufacturer's instructions. cDNA was synthesized and amplified with Smart-Seq v4 Ultra Low input RNA kit (Clontech) according to the kit manual. Total RNA extraction from murine primary HSCs and freshly isolated hepatocytes and quantitative PCR were performed as described above. Primers used were as follows: mouse *Gapdh,* 5′-CAACTACATGGTC TACATGTTC-3′ (forward) and 5′-CACCAGTAGACTCCACGAC-3′ (reverse); mouse *Ptger4*, 5′-TGCTCCATTCCGCTCGT-3′ (forward) and 5′-GCACAGTCTTCCGAAGAAGG-3′ (reverse).

Human Subjects

Written informed consent was obtained from all patients according to the protocol reviewed and approved by the board members of the ethics committee of the Japanese Foundation for Cancer Research (JFCR) in accordance with the Declaration of Helsinki. The protocols for the analysis of human liver samples were also reviewed and approved by the board members of the ethics committee of the Tokyo University of Science in accordance with the Declaration of Helsinki.

Statistical Analysis

Data were analyzed by an unpaired *t* test with Welch correction (two-sided) or the Mann–Whitney test (two-sided). *P* values less than 0.05 were considered statistically significant. "NS" indicates not significant.

Disclosure of Potential Conflicts of Interest

S. Narumiya is a consultant/advisory board member for Astellas Pharma. No potential conflicts of interest were disclosed by the other authors.

Authors' Contributions

Conception and design: T.M. Loo, F. Kamachi, M.M. Taketo, N. Ohtani

Development of methodology: T.M. Loo, F. Kamachi, S. Yoshimoto, Y. Arai, A. Iwama, S. Narumiya, M. Arita, N. Ohtani

Acquisition of data (provided animals, acquired and managed patients, provided facilities, etc.): T.M. Loo, F. Kamachi, Y. Watanabe, H. Kanda, Y. Arai, A. Iwama, Y. Sugimoto, M. Nakamura, M. Kumagai, M.M. Taketo, M. Arita, N. Ohtani

Analysis and interpretation of data (e.g., statistical analysis, biostatistics, computational analysis): T.M. Loo, F. Kamachi, S. Yoshimoto, Y. Arai, T. Ozawa, S. Narumiya, M. Arita, E. Hara, N. Ohtani

Writing, review, and/or revision of the manuscript: T.M. Loo, F. Kamachi, M. Arita, N. Ohtani

Administrative, technical, or material support (i.e., reporting or organizing data, constructing databases): Y. Nakajima-Takagi, T. Koga, K. Watashi, T. Aoki, S. Narumiya, M. Oshima, N. Ohtani

Study supervision: F. Kamachi, E. Hara, N. Ohtani

Acknowledgments

The authors thank the Jei-ei-shi staff for technical support and animal care, Tatsuya Ando and Tatsuhiro Kubota for their assistance in primary cell culture, and the Ohtani lab members for their technical support and useful discussion.

Grant Support

This work was supported in part by Grant in Aid for Scientific Research on Innovative Areas from MEXT, Japan, #26115005 (N. Ohtani, "Stem cell aging and disease"), #15H05898 (M. Arita, "Quality of lipids in biological systems"), JSPS KAKENHI #16H04699 (N. Ohtani), #15K19031 (F. Kamachi), #26713014 (S. Yoshimoto), #26250028 (E. Hara), #15H04648 (M. Arita), Precursory Research for Embryonic Science and Technology (PRESTO) from the Japan Science and Technology Corporation (JST), 10104022 (N. Ohtani), and AMED, Japan Agency for Medical Research and Development, Japan, 15654813 (N. Ohtani). T.M. Loo was supported in part by a fellowship and a grant from the Japan Society for Promotion of Science (JSPS; 14J0-6998).

This work was also supported by the Yakult Bio-science Foundation (N. Ohtani) and the Ono Medical Research Foundation (N. Ohtani).

The costs of publication of this article were defrayed in part by the payment of page charges. This article must therefore be hereby marked *advertisement* in accordance with 18 U.S.C. Section 1734 solely to indicate this fact.

Received August 22, 2016; revised February 13, 2017; accepted February 13, 2017; published OnlineFirst February 15, 2017.

REFERENCES

1. Calle EE, Kaaks R. Overweight, obesity and cancer: epidemiological evidence and proposed mechanisms. Nat Rev Cancer 2004;4:579–91.
2. Deng T, Lyon CJ, Bergin S, Caligiuri MA, Hsueh WA. Obesity, inflammation, and cancer. Annu Rev Pathol 2016;11:421–49.
3. Font-Burgada J, Sun B, Karin M. Obesity and cancer: the oil that feeds the flame. Cell Metab 2016;23:48–62.
4. Yoshimoto S, Loo TM, Atarashi K, Kanda H, Sato S, Oyadomari S, et al. Obesity-induced gut microbial metabolite promotes liver cancer through senescence secretome. Nature 2013;499:97–101.
5. Forner A, Llovet JM, Bruix J. Hepatocellular carcinoma. Lancet 2012;379:1245–55.
6. Michelotti GA, Machado MV, Diehl AM. NAFLD, NASH and liver cancer. Nat Rev Gastroenterol Hepatol 2013;10:656–65.
7. Rodier F, Campisi J. Four faces of cellular senescence. J Cell Biol 2011;192:547–56.
8. Campisi J, Andersen JK, Kapahi P, Melov S. Cellular senescence: a link between cancer and age-related degenerative disease? Semin Cancer Biol 2011;21:354–9.
9. Collado M, Serrano M. Senescence in tumours: evidence from mice and humans. Nat Rev Cancer 2010;10:51–7.
10. Munoz-Espin D, Canamero M, Maraver A, Gomez-Lopez G, Contreras J, Murillo-Cuesta S, et al. Programmed cell senescence during mammalian embryonic development. Cell 2013;155:1104–18.
11. Storer M, Mas A, Robert-Moreno A, Pecoraro M, Ortells MC, Di Giacomo V, et al. Senescence is a developmental mechanism that contributes to embryonic growth and patterning. Cell 2013;155:1119–30.
12. Kang TW, Yevsa T, Woller N, Hoenicke L, Wuestefeld T, Dauch D, et al. Senescence surveillance of pre-malignant hepatocytes limits liver cancer development. Nature 2011;479:547–51.
13. Krizhanovsky V, Yon M, Dickins RA, Hearn S, Simon J, Miething C, et al. Senescence of activated stellate cells limits liver fibrosis. Cell 2008;134:657–67.
14. Tasdemir N, Banito A, Roe JS, Alonso-Curbelo D, Camiolo M, Tschaharganeh DF, et al. BRD4 connects enhancer remodeling to senescence immune surveillance. Cancer Discov 2016;6:612–29.
15. Demaria M, Ohtani N, Youssef SA, Rodier F, Toussaint W, Mitchell JR, et al. An essential role for senescent cells in optimal wound healing through secretion of PDGF-AA. Dev Cell 2014;31:722–33.
16. Jun JI, Lau LF. The matricellular protein CCN1 induces fibroblast senescence and restricts fibrosis in cutaneous wound healing. Nat Cell Biol 2010;12:676–85.
17. Acosta JC, Banito A, Wuestefeld T, Georgilis A, Janich P, Morton JP, et al. A complex secretory program orchestrated by the inflammasome controls paracrine senescence. Nat Cell Biol 2013;15:978–90.
18. Pribluda A, Elyada E, Wiener Z, Hamza H, Goldstein RE, Biton M, et al. A senescence-inflammatory switch from cancer-inhibitory to cancer-promoting mechanism. Cancer Cell 2013;24:242–56.
19. Cichowski K, Hahn WC. Unexpected pieces to the senescence puzzle. Cell 2008;133:958–61.
20. Kang C, Xu Q, Martin TD, Li MZ, Demaria M, Aron L, et al. The DNA damage response induces inflammation and senescence by inhibiting autophagy of GATA4. Science 2015;349:aaa5612.
21. Kaplon J, Zheng L, Meissl K, Chaneton B, Selivanov VA, Mackay G, et al. A key role for mitochondrial gatekeeper pyruvate dehydrogenase in oncogene-induced senescence. Nature 2013;498:109–12.
22. Rai TS, Cole JJ, Nelson DM, Dikovskaya D, Faller WJ, Vizioli MG, et al. HIRA orchestrates a dynamic chromatin landscape in senescence and is required for suppression of neoplasia. Genes Dev 2014;28:2712–25.
23. Takahashi A, Imai Y, Yamakoshi K, Kuninaka S, Ohtani N, Yoshimoto S, et al. DNA damage signaling triggers degradation of histone methyltransferases through APC/C(Cdh1) in senescent cells. Mol Cell 2012;45:123–31.
24. Vigneron A, Vousden KH. p53, ROS and senescence in the control of aging. Aging 2010;2:471–4.
25. Davalos AR, Kawahara M, Malhotra GK, Schaum N, Huang J, Ved U, et al. p53-dependent release of Alarmin HMGB1 is a central mediator of senescent phenotypes. J Cell Biol 2013;201:613–29.
26. Dapito DH, Mencin A, Gwak GY, Pradere JP, Jang MK, Mederacke I, et al. Promotion of hepatocellular carcinoma by the intestinal microbiota and TLR4. Cancer Cell 2012;21:504–16.
27. Ley RE, Turnbaugh PJ, Klein S, Gordon JI. Microbial ecology: human gut microbes associated with obesity. Nature 2006;444:1022–3.
28. Fukui H. Gut-liver axis in liver cirrhosis: How to manage leaky gut and endotoxemia. World J Hepatol 2015;7:425–42.
29. Goodman ZD. The impact of obesity on liver histology. Clin Liver Dis 2014;18:33–40.
30. Arita M. Mediator lipidomics in acute inflammation and resolution. J Biochem 2012;152:313–9.
31. Morita M, Kuba K, Ichikawa A, Nakayama M, Katahira J, Iwamoto R, et al. The lipid mediator protectin D1 inhibits influenza virus replication and improves severe influenza. Cell 2013;153:112–25.
32. Schwab JM, Chiang N, Arita M, Serhan CN. Resolvin E1 and protectin D1 activate inflammation-resolution programmes. Nature 2007;447:869–74.
33. Castellone MD, Teramoto H, Williams BO, Druey KM, Gutkind JS. Prostaglandin E2 promotes colon cancer cell growth through a Gs-axin-beta-catenin signaling axis. Science 2005;310:1504–10.
34. Oshima H, Matsunaga A, Fujimura T, Tsukamoto T, Taketo MM, Oshima M. Carcinogenesis in mouse stomach by simultaneous activation of the Wnt signaling and prostaglandin E2 pathway. Gastroenterology 2006;131:1086–95.
35. Wang D, Dubois RN. Eicosanoids and cancer. Nat Rev Cancer 2010;10:181–93.
36. Harris SG, Padilla J, Koumas L, Ray D, Phipps RP. Prostaglandins as modulators of immunity. Trends Immunol 2002;23:144–50.
37. Chen JH, Perry CJ, Tsui YC, Staron MM, Parish IA, Dominguez CX, et al. Prostaglandin E2 and programmed cell death 1 signaling coordinately impair CTL function and survival during chronic viral infection. Nat Med 2015;21:327–34.
38. Soontrapa K, Honda T, Sakata D, Yao C, Hirata T, Hori S, et al. Prostaglandin E2-prostaglandin E receptor subtype 4 (EP4) signaling mediates UV irradiation-induced systemic immunosuppression. Proc Natl Acad Sci U S A 2011;108:6668–73.
39. Fuertes MB, Kacha AK, Kline J, Woo SR, Kranz DM, Murphy KM, et al. Host type I IFN signals are required for antitumor CD8+ T cell responses through CD8{alpha}+ dendritic cells. J Exp Med 2011;208:2005–16.
40. Zelenay S, van der Veen AG, Bottcher JP, Snelgrove KJ, Rogers N, Acton SE, et al. Cyclooxygenase-dependent tumor growth through evasion of immunity. Cell 2015;162:1257–70.
41. Perumpail RB, Wong RJ, Ahmed A, Harrison SA. Hepatocellular carcinoma in the setting of non-cirrhotic nonalcoholic fatty liver disease and the metabolic syndrome: US Experience. Dig Dis Sci 2015;60:3142–8.
42. Takuma Y, Nouso K. Nonalcoholic steatohepatitis-associated hepatocellular carcinoma: our case series and literature review. World J Gastroenterol 2010;16:1436–41.
43. Forman D, Ferlay J. The global and regional burden of cancer. In: Stewart Bernard W, Wild Christpher L, editors. World Cancer Report 2014. World Health Organization; 2014. p.16–53.
44. Sawey ET, Chanrion M, Cai C, Wu G, Zhang J, Zender L, et al. Identification of a therapeutic strategy targeting amplified FGF19 in liver cancer by Oncogenomic screening. Cancer Cell 2011;19:347–58.
45. Wang L, Fouts DE, Starkel P, Hartmann P, Chen P, Llorente C, et al. Intestinal REG3 lectins protect against alcoholic steatohepatitis

by reducing mucosa-associated microbiota and preventing bacterial translocation. Cell Host Microbe 2016;19:227–39.
46. Miura K, Ohnishi H. Role of gut microbiota and Toll-like receptors in nonalcoholic fatty liver disease. World J Gastroenterol 2014; 20:7381–91.
47. Bauer CA, Kim EY, Marangoni F, Carrizosa E, Claudio NM, Mempel TR. Dynamic Treg interactions with intratumoral APCs promote local CTL dysfunction. J Clin Invest 2014;124:2425–40.
48. Joyce JA, Fearon DT. T cell exclusion, immune privilege, and the tumor microenvironment. Science 2015;348:74–80.
49. Okumura Y, Yamagishi T, Nukui S, Nakao K. Discovery of AAT-008, a novel, potent, and selective prostaglandin EP4 receptor antagonist. Bioorg Med Chem Lett 2017;27:1186–92.
50. Kurtova AV, Xiao J, Mo Q, Pazhanisamy S, Krasnow R, Lerner SP, et al. Blocking PGE2-induced tumour repopulation abrogates bladder cancer chemoresistance. Nature 2015;517:209–13.